https://doi.org/10.1007/s41230-025-4177-z

Designing the counter pressure casting gating system for a large thin-walled cabin by machine learning

Xiao-long Zhang[1], *Hua Hou[1], Xiao-long Pei[1], Zhi-qiang Duan[1], and **Yu-hong Zhao[1, 2, 3]

1. School of Materials Science and Engineering, Collaborative Innovation Center of Ministry of Education and Shanxi Province for High-performance Al/Mg Alloy Materials, North University of China, Taiyuan 030051, China

2. Beijing Advanced Innovation Center for Materials Genome Engineering, University of Science and Technology Beijing, Beijing 100083, China

3. Institute of Materials Intelligent Technology, Liaoning Academy of Materials, Shenyang 110004, China

Abstract: The design of casting gating system directly determines the solidification sequence, defect severity, and overall quality of the casting. A novel machine learning strategy was developed to design the counter pressure casting gating system of a large thin-walled cabin casting. A high-quality dataset was established through orthogonal experiments combined with design criteria for the gating system. Spearman's correlation analysis was used to select high-quality features. The gating system dimensions were predicted using a gated recurrent unit (GRU) recurrent neural network and an elastic network model. Using EasyCast and ProCAST casting software, a comparative analysis of the flow field, temperature field, and solidification field can be conducted to demonstrate the achievement of steady filling and top-down sequential solidification. Compared to the empirical formula method, this method eliminates trial-and-error iterations, reduces porosity, reduces casting defect volume from 11.23 cubic centimeters to 2.23 cubic centimeters, eliminates internal casting defects through the incorporation of an internally cooled iron, fulfilling the goal of intelligent gating system design.

Keywords: machine learning; large thin-walled cabin; gating system design; GRU recurrent neural network

CLC numbers: TG249.9/TP18 **Document code:** A **Article ID:** 1672-6421(2025)04-395-12

1 Introduction

Counter pressure casting, a type of anti-gravity casting, plays a critical role in diverse industrial sectors, particularly in aviation, defense, and railway manufacturing [1-2]. The casting process involves two primary stages: mold filling with molten metal and subsequent solidification. Inadequate design of the gating system or improper pouring methods can lead to severe defects, significantly compromising casting quality. These defects may include shrinkage cavities, porosity, and cold shuts [3-9].

Current mainstream research utilizes empirical formulas to determine gating system dimensions in conjunction with computer numerical simulations to optimize process parameters and predict potential defects. This approach seeks to establish optimal process plans and reduce casting production costs [10-11]. Jiang et al. [12] developed three optimized gating system designs based on trial production results of a support component. They further refined the gating system parameters through numerical simulations, ultimately determining the optimal pouring process that was subsequently validated in actual production. Wang et al. [13] designed a combination of bottom injection and slit gating system for low-pressure casting of aluminum alloy thin-walled shells, employing numerical simulation and other means to optimize the casting process parameters. The results showed that the optimized aluminum alloy thin-walled shells were free of shrinkage and porosity defects and

***Hua Hou**

Ph. D., Professor. Research interests: Intelligent design and optimization of casting process, macro and micro numerical simulation of casting process, design and preparation technology of non-ferrous metal materials.

E-mail: houhua@nuc.edu.cn

****Yu-hong Zhao**

Ph. D., Professor. Research interests: Application of multi-scale physical modeling and data-driven approaches in alloy design and forming optimization, prediction of solidification and aging microstructure in liquid metal forming.

E-mail: zhaoyuhong@nuc.edu.cn

Received: 2024-08-22; Revised: 2024-10-27; Accepted: 2024-11-15

the mechanical properties of the castings were significantly improved. Andrzej et al. [14] improved an existing gating system using MAGMAsoft software for casting process simulation. This approach enabled optimization of process parameters, which were subsequently validated through experiments, demonstrating their suitability for industrial production.

To meet the demands of industrial production, counter pressure casting processes require high precision, high efficiency, and intelligent design [15]. However, the traditional approach of iteratively modifying the gating system to eliminate potential casting defects often results in inefficient trial-and-error cycles [16]. Furthermore, traditional empirical formula methods fail to adequately address the design of straight sprue diameter dimensions in slit gating system for counter pressure casting [17-19]. The basic concept of material genetic engineering is to change the traditional "trial-and-error" research mode. Instead, it aims to develop a new R&D paradigm that deeply integrates "rational design", "efficient experimentation", and "big data technology", along with collaborative innovation [20]. Building upon this concept, the integration of domain-specific material knowledge with machine learning techniques enables the construction of data-driven models. These models, incorporating big data analysis, design, and prediction capabilities, offer innovative approaches to material processing [21].

Zhou et al. [22] developed a two-stage optimization process for counter pressure casting of steering knuckles. In the first stage, they employed group simulation techniques to identify key parameters influencing casting quality. Subsequently, they utilized a hybrid approach combining back-propagation neural networks and the artificial fish swarm algorithm to determine optimal process parameters that minimize defects. Yu et al. [23] developed a data-driven framework to optimize gating systems in investment casting. Utilizing a radial basis function optimization algorithm, they designed an efficient gating system that simultaneously reduced porosity defects and improved yield in castings. Wang et al. [24] developed a gating system optimization method using a fruit fly algorithm-based casting simulation technology. They established a geometric model of the gating system. Furthermore, they optimized the dimensions of the upper center plate gating system using the fruit fly optimization algorithm. Experimental results demonstrated reduced surface porosity and elimination of internal porosity in the castings.

However, the accuracy of machine learning models is dependent on dataset quality, with the current research often aiming to address quality issues by increasing data quantity [25-27]. But, in the field of casting, both the experimental and the simulation approaches are extremely time-consuming [28-29]. Furthermore, given the multitude of parameters involved in gating system design, the judicious selection of appropriate machine learning models is crucial [30]. In this study, the process parameters range from previous counter pressure casting literature were referenced. Traditional empirical formulas were used to calculate the range of the sizes of gating system, while design guidelines for closed gating systems were employed to determine the straight sprue sizes. An orthogonal method was utilized to construct a high-quality dataset. The porosity, pouring temperature, and filling pressure served as inputs to the model, with the straight sprue size, inner gate size, and number of sprues being the prediction objects. These parameters were used to find the optimal values by constructing a gated recurrent unit (GRU) model and an elastic network model for prediction. The flow field, solidification process, and shrinkage distribution were compared and analyzed using EasyCast and ProCAST software for gating systems designed by the empirical method and those optimized by the machine learning model. The model's performance was evaluated using the mean squared error (MSE) and the coefficient of determination.

2 Characteristics of castings and research methodology

This study employs machine learning techniques to design the gating system dimensions for a large-scale thin-walled cabin. As shown in Fig. 1, the conical casting has the sizes of Φ317 mm×544 mm and a height of 806 mm. It has a complex internal structure with many tabs and reinforcement bars, and the average wall thickness is around 15 mm. The material selected is ZL101.

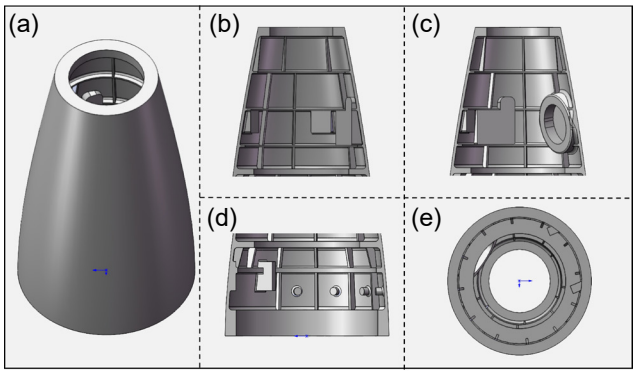

Fig. 1: Conical casting (a) and its sectional (b–d) and top (e) views

This study proposes a strategy that integrates empirical design with machine learning to optimize the dimensioning of the gating system. The detailed framework is illustrated in Fig. 2. The strategy is based on empirical formulations and numerical simulations. High-quality datasets were established through orthogonal experiments, and features were screened using Spearman correlation analysis. Models were constructed and gating system dimensions were predicted based on GRU and elastic networks. Subsequently, defect distributions were analyzed using numerical simulation software.

2.1 Data collection

A high-quality dataset is fundamental for achieving high accuracy in machine learning models [30]. In order to ensure that the machine learning model can effectively capture the nonlinear relationships between inputs and outputs, this study will acquire data through the following three steps.

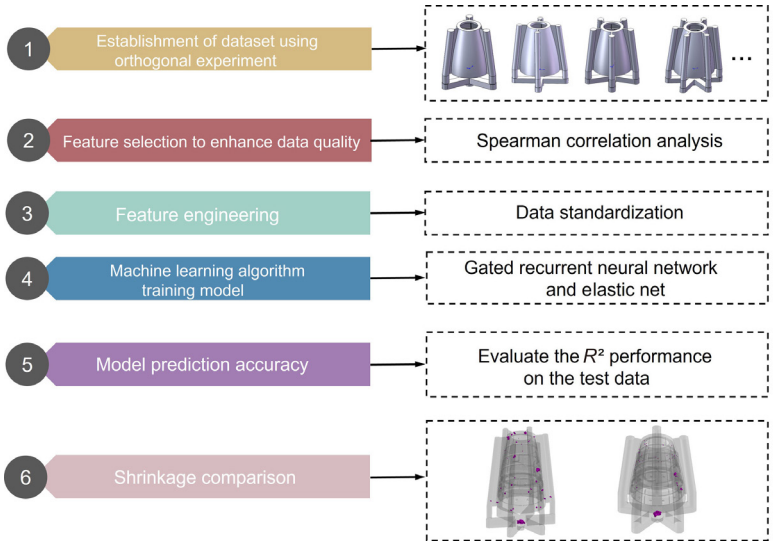

Fig. 2: Schematic of machine learning workflow

2.1.1 Literature statistics

To gather relevant data for this study, a literature review of recent counterpressure casting research was conducted, focusing on castings with a height of approximately 800 mm. The casting process parameter values were statistically analyzed and verified to ensure accuracy. Data completeness was ensured through appropriate data expansion techniques to fill any gaps in the dataset. The specific ranges of the casting process parameters are presented in Table 1.

Table 1: Process parameters and their ranges

Filling pressure (kPa)	Crystallization booster pressure (kPa)	Crystallization time (s)	Pouring temperature (°C)
40–70	40–70	300–600	680–710

2.1.2 Design of gating system dimensional data by empirical methods

Usually, the parameters of the slot gating system are calculated according to the following empirical equations [31]:

$$n = (0.016–0.028)S/\delta \quad (1)$$

$$\delta = (0.8–1.5)S/\delta_{casting} \quad (2)$$

$$b = 15–35\ \text{mm} \quad (3)$$

$$d = (4–6)\delta \quad (4)$$

where

n: the number of sprues;

S: the circumference of the casting shape;

δ: the thickness of the inner gate in the gap;

b: the width of the inner gate in the gap;

d: the diameter of the inner gate.

For anti-gravity casting, the inner gate not only imports the metal liquid but also plays the role of feeding. To determine the cross-sectional area of the inner gate during the design phase, the riser calculation method was employed [32]. For the aluminum alloy ZL101, which is commonly used in anti-gravity casting, the design guidelines for a closed gating system are as following:

$$\sum A_g < \sum A_{ru} < \sum A_{straight\ sprue} \quad (5)$$

$\sum A_g$: inner gate cross-sectional area;

$\sum A_{ru}$: cross-sectional area of the horizontal runner;

$\sum A_{straight\ sprue}$: cross-sectional area of the straight sprue.

By using the above Eqs. (1) to (4), three parameters: number of sprues, straight sprue diameter, and inner gate diameter were selected as part of the data set for this study, with the specific ranges shown in Table 2.

Table 2: Range of gating system size

Number of sprues	Inner gate diameter	Straight sprue diameter
3–6	60–90 mm	Determined by closed gating system design guidelines

2.1.3 Construction of data sets using orthogonal tables

The number of sprues is between 3 and 6 calculated according to the empirical design method mentioned above. Therefore, only 28 groups of data could be established using an orthogonal experiments at the 7-factors and 4-levels. To prevent the overfitting phenomenon caused by an insufficient amount of data, a mixed orthogonal table (77 groups) was employed. As shown in Table 3, 77 groups of data were established by 7-factor mixing level, and then the corresponding defect volume as well as other variables (casting volume, filling

Table 3: Example of a mixed orthogonal table

Factors / Levels	HTC ($W \cdot m^{-2} \cdot K^{-1}$)	Filling pressure (kPa)	Crystallization booster pressure (kPa)	Pouring temperature (°C)	Holding time (s)	Number of sprues	Inner gate diameter (mm)
L-1	750	40	40	680	300	3	60
L-2	900	45	45	690	350	4	65
L-3	1,000	50	50	700	400	5	70
L-4	2,000	55	55	710	450	6	75
L-5		60	60		500		80
L-6		65	65		550		85
L-7		70	70		600		90

time, etc.) were obtained by group simulation and simulation calculation for each group of experiments.

The overfitting phenomenon can be effectively reduced by the mixed orthogonal experiment established by selecting seven levels of the four factors, namely, filling pressure, crystallization booster pressure, holding time, and inner gate diameter. In combination with numerical simulations and general rules for the design of closed gating systems, a high-quality dataset can be created that allows for efficient parametric design.

2.2 Feature screening

High-quality features provide more accurate and comprehensive information, which can improve model accuracy. Therefore, feature selection is necessary to eliminate irrelevant or redundant features. Since the relationship between features and the target variable is often nonlinear, Spearman's correlation coefficient, which can capture nonlinear relationships, was chosen for feature selection. Spearman's correlation analysis assumes that two random variables, X and Y, with the same number of elements N, are considered. The ith ($1 \le i \le n$) value is randomly selected and denoted by x_i, y_i respectively. Sorting X and Y yields two ranked sets x and y, where elements x_i, y_i represent the rankings of X_i in X and Y_i in Y, respectively. The Spearman's correlation coefficient (ρ) between the random variables X and Y can be calculated using the ranking differences, denoted as d [33]. The equation for computing ρ is as follows:

$$\rho = 1 - \frac{6\sum d_i^2}{n\left(n^2-1\right)} \tag{6}$$

where d_i denotes the rank difference between X_i and Y_i; n represents the total number of observed samples.

2.3 Model selection and construction

In this study, different models were used for prediction based on the characteristics of data distribution.

2.3.1 GRU model

For the case of more uniform data distribution, the gated recurrent unit (GRU) model was selected for prediction. GRU, is a variant of recurrent neural networks. Compared with traditional RNN and LSTM, GRU has lower computational complexity and fewer parameters [34], and during the training process, parameters such as learning rate can be adjusted to make the training of the model easier. Figure 3 shows the internal unit structure in GRU, where h_{t-1} is the hidden state at the previous moment, h_t is the hidden state output at the current moment, $\tilde{h}_t$ is candidate hidden state, and x_t is the data input at the current moment [34].

The specific forward propagation equations are as follows [34]:

$$r_t = \sigma\left(W_{\mathrm{xr}} x_t + W_{\mathrm{hr}} h_{t-1} + b_r\right) \tag{7}$$

$$z_t = \sigma\left(W_{\mathrm{xz}} x_t + W_{\mathrm{hz}} h_{t-1} + b_z\right) \tag{8}$$

$$\tilde{h}_t = \tanh\left(W_{\mathrm{xh}} x_t + W_{\mathrm{hh}}\left(r_t \odot h_{t-1}\right) + b_h\right) \tag{9}$$

$$h_t = z_t h_{t-1} + \left(1 - z_t\right) \odot \tilde{h}_t \tag{10}$$

W_{xr}: weight matrix of the input layer to the update gate;
W_{hr}: weight matrix of the hidden state to the update gate;
W_{xz}: weight matrix of the input layer to the reset gate;
W_{hz}: weight matrix from hidden state to reset gate;
W_{xh}: weight matrix of input layer to hidden states;
W_{hh}: weight matrix of connections between hidden states;
σ: can transform data into values within the range of 0 to 1;
tan$h$: can transform data into values within the range of –1 to 1;
b_r, b_z, b_h: are the bias vectors of the hidden units of the

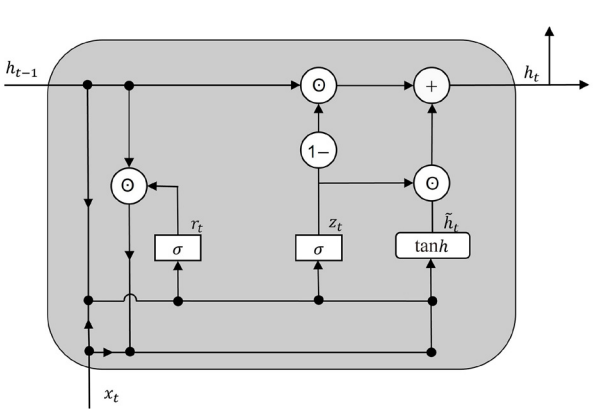

Fig. 3: Internal structure of GRU

update gate and the reset gate, respectively.

Furthermore, r_t is the reset gate, which determines how the new input information is combined with the previous memory. The smaller the value of r_t, the more the previous moment needs to be forgotten and the more it is discarded. z_t is the update gate, which is used to control the extent to which the previous moment's state information has been brought into the current state. When z_t is close to 1, it indicates that more data have been "remembered"; conversely, when z_t is close to 0, it signifies that more data have been "forgotten".

2.3.2 Elastic networks

Elastic network is a linear regression algorithm that combines two regularization methods, Lasso (L1 regularization) and Ridge regression (L2 regularization) [35]. Its main purpose is to avoid problems such as overfitting and unsolvability while retaining the advantages of linear regression (simple and effective linear model). This suits for prediction of straight sprue in this study.

The elastic network controls the complexity of the model by introducing L1 and L2 regularization terms in the loss function, and balances the weights of these two regularization terms in the optimization process. Among them, the L1 regularization term can reduce some unimportant feature coefficients to 0 and play the role of feature selection; while the L2 regularization term can smooth the weight of the coefficients to prevent the coefficients from varying too drastically, which has a certain degree of noise reduction ability.

The elastic network regression problem can be solved by the following equation:

$$\hat{\beta}=\arg\min\left\{\sum_{i=1}^{N}\left(y_i-\beta_0-\sum_{j=1}^{p}x_{ij}\beta_j\right)^2+\lambda_1\sum_{j=1}^{p}\left|\beta_j\right|+\lambda_1\sum_{j=1}^{p}\beta_j^2\right\} \tag{11}$$

$\hat{\beta}$: the coefficient vector of the elastic net regression estimator;

y_i: the actual value of the target variable for the ith observation;

β_0: the intercept term in the regression model;

x_{ij}: the jth feature value for the –ith observation;

β_j: the coefficient corresponding to the –jth feature;

N: the total number of observations in the dataset;

p: the total number of features (or predictors) in the model;

λ_1 and λ_2: the penalty parameters.

When λ_1=0 and λ_2=0, the regression model is least squares regression; when 1=0 and λ_2>0, the regression model is Ridge regression; when λ_1>0 and λ_2=0, the regression model is Lasso regression; and when λ_1>0 and λ_2>0, the regression model is elastic network regression [36].

2.3.3 Modeling

To eliminate the effects of different features due to different attributes, the data are standardized to make it dimensionless. The specific standardization equation is as follows:

$$x_n=\frac{x_i-\mu}{\sigma} \tag{12}$$

where μ is the sample mean, σ is the sample standard deviation, x_i is the original data, and x_n is the transformed data.

The dataset is partitioned into training and validation sets using a 4:1 ratio. The model accuracy is evaluated using the mean squared error (MSE) and the coefficient of determination (R^2). The specific equation is given below:

$$\mathrm{MSE}=\frac{1}{n}\sum_{i=1}^{n}\left(Y_{\mathrm{true}}-Y_{\mathrm{pre}}\right)^2 \tag{13}$$

$$R^2=1-\frac{\sum_{i=1}^{n}\left(Y_{\mathrm{true}}-Y_{\mathrm{pre}}\right)^2}{\sum_{i=1}^{n}\left(\bar{Y}-Y_{\mathrm{true}}\right)^2} \tag{14}$$

where Y_{true} is the true value of the sample, Y_{pre} is the predicted value of the model, and $\bar{Y}$ is the sample mean. The smaller the value of MSE, the smaller the difference between the predicted value of the model and the true value, the better the performance of the model.

The model is built based on GRU and deep neural networks (DNN). The number of units in the GRU layer is set to 100. Input data are organized in sequences of 7-time steps, where each sequence captures information spanning 7-time steps. This means that the model will receive a feature value at each time step and process the input sequence after 7-time steps. The feature dimension of the input sequence at each time step is 2 (i.e., the output at that moment). Then, after obtaining the hidden layer output of the last time step of the GRU module, it is fed into the DNN to perform dimension transformation. This process firstly increases the network output dimension from 100 to 128, then, reduces it from 128 to 64, and finally, decreases it to the output dimension of 2. In order to enhance the learning ability of the model, it is possible to appropriately increase the number of DNN layers, and to use the rectified linear unit (ReLU) as the activation function of the hidden layer to improve the learning efficiency.

The structure of the final constructed GRU-DNN model is shown in Fig. 4, where x_t is the input for time step t; h_t^l is the hidden state of the GRU module at time step t; d_t^l is the ith hidden unit of the lth layer of the DNN module; f_{ReLU}=max(x, 0) is a linear activation function. It serves to limit the input values to non-negative ranges and has a linear nature on the positive semi-axis, which can enhance the model nonlinear capability.

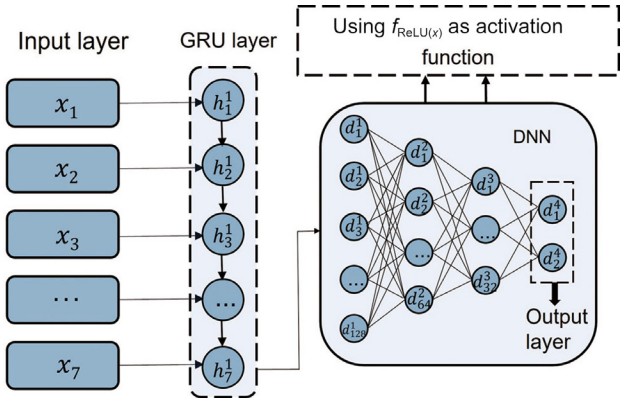

Fig. 4: GRU-DNN model

For the prediction of the straight sprue, an elastic network model was used to find the optimal parameters by searching the hyperparameters through a grid search, as shown in Table 4.

Table 4: Choosing the best hyperparameters for elastic network

Hyperparameter	Hyperparameter range	Optimal hyperparameters
alpha	[0.01, 0.1, 0.15, 0.5, 0.75, 1]	0.15
L1_ratio	[0.001, 0.01, 0.1, 0.5, 0.75, 1]	False
fit_intercept	[True, false]	0.01
max_iter	[1,000; 1,500; 2,000; 2,500; 3,000]	2,000

Grid search is a method that, by traversing all permutations of the input parameters, returns the evaluation metric scores for all parameter combinations through cross-validation. In this model, a value of 0.15 for alpha indicates a smaller regularization strength. fit_intercept of false indicates that the model will not learn the intercept and the fitted line will pass through the origin. When L1_ratio is 1, the model uses only L1 regularization (Lasso) and when L1_ratio is 0, the model uses only L2 regularization (Ridge). In this model, a value of 0.01 for L1_ratio indicates a smaller percentage of L1 regularization. The maximum number of iterations for model training is 2,000.

3 Results and analysis

3.1 Model accuracy

Following model optimization, the coefficient of determination (R^2) was used to assess the model accuracy. As shown in Figs. 5 and 6, the training and predicted data are centered around $Y=X$, and the R^2 values for the outputs (straight sprue diameter, inner gate diameter, number of sprues) are: 0.982, 0.856, and 0.820. This indicates that the model is well fitted and has good predictive ability for the target variables. For the straight sprue diameter, the predicted R^2 value is only 0.82, and the reasons for this relatively low value are analyzed as follows: (1) The dataset size: the small number of datasets may not fully capture the nonlinear relationship between the input features and the straight sprue diameter; (2) The features used in this study may be more suitable for predicting the number of sprues or the inner gate diameter, but less effective for predicting the straight sprue diameter.

3.2 Grid independence verification and method analysis

3.2.1 Grid independence verification

Grid independence verification is essential to ensure the reliability and reproducibility of results in numerical simulations. Therefore, a grid independence analysis was performed to determine the appropriate number of meshes for maintaining computational accuracy. As shown in Tables 5 and 6, when the number of volume mesh elements is increased from 1.7 million to 5.2 million, the changes in porosity and defect volume of the castings remain relatively stable. To balance simulation efficiency and accuracy, subsequent calculations employ the mesh configuration of Case 3, with the final grid chart depicted in Fig. 7.

3.2.2 Comparative analysis of the methods

To evaluate the model's predictive performance, the dimensions of the gating system for this casting were compared with those obtained using empirical formulas. The same process parameters were used as inputs for both the model and the empirical method. The model's predicted gating system dimensions are then compared with the results calculated using the empirical formulas. EasyCast [7] and ProCAST casting numerical simulation softwares were used to calculate the flow field, solidification field, and defect distribution. EasyCast software utilizes the finite difference method to calculate heat transfer and volume changes, enhancing the accuracy of predictions for casting shrinkage and porosity [13]. The specific parameters are shown in Tables 7 and 8.

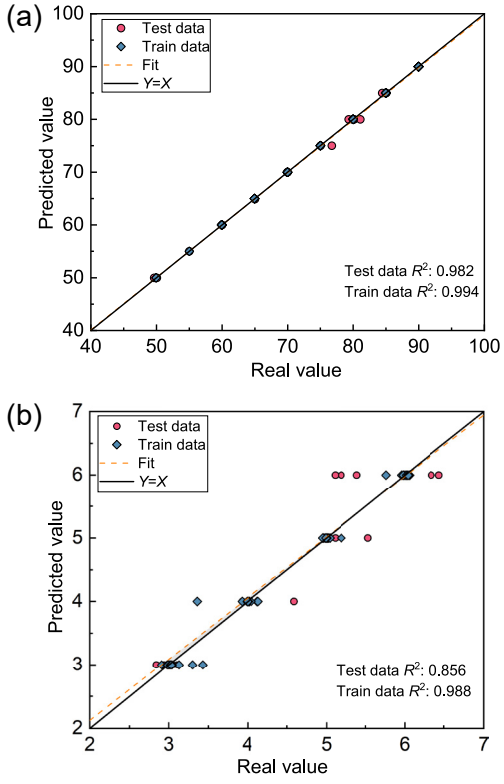

Fig. 5: Prediction accuracy of the GRU model: (a) inner gate diameter; (b) number of sprue

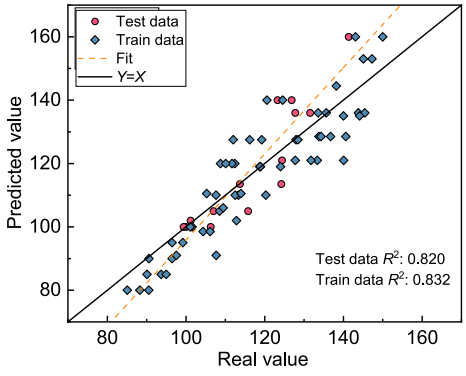

Fig. 6: Prediction of straight sprue diameter by elastic net

Table 5: Independence verification of grid with empirical formula approach

Cases	Number of surface grids	Number of volume grids	Porosity (%)	Defect volume (cm^3)
1	56,471	602,869	1.527	7.05
2	105,344	1,041,169	2.573	4.68
3	130,450	1,749,456	3.143	2.06
4	288,694	5,193,869	3.175	2.23

Table 6: Independence verification of grid with machine learning models

Cases	Number of surface grids	Number of volume grids	Porosity (%)	Defect volume (cm^3)
1	55,366	606,367	1.986	16.576
2	106,894	1,100,698	2.974	13.257
3	133,126	1,784,446	3.358	11.238
4	305,672	5,272,561	3.381	11.457

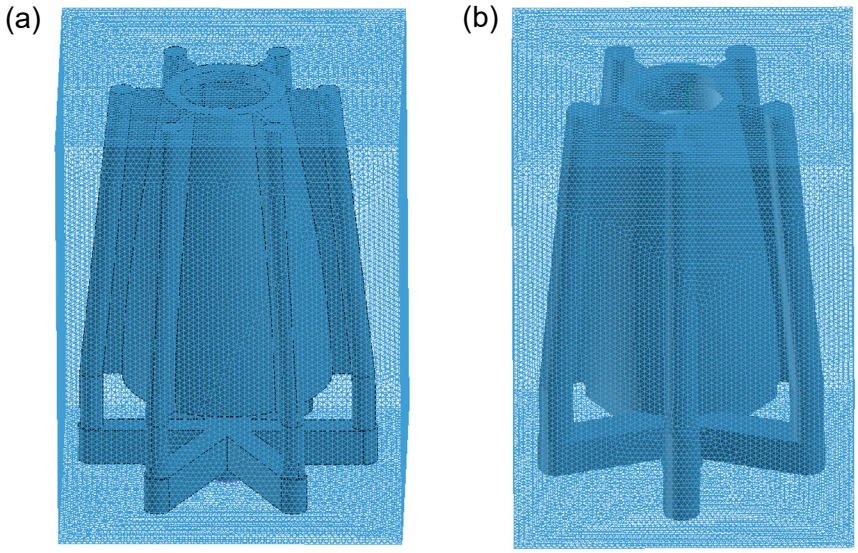

Fig. 7: Empirical formula approach (a) and machine learning models (b)

Table 7: Counter pressure casting process parameters

Lifting pressure (kPa)	Lifting time (s)	Filling pressure (kPa)	Filling time (s)	Crust pressurization pressure (kPa)	Crystallization booster pressure (kPa)	Holding time (s)	Pouring temperature (°C)	HTC ($W \cdot m^{-2} \cdot K^{-1}$)
15	15	55	7	4	40	300	700	2,000

Table 8: Design of gating system dimensions using empirical formulations and model prediction

Methods	Number of sprue	Inner gate diameter (mm)	Straight sprue diameter (mm)
Empirical formulations	6	60	80
Model prediction	4.79 (5)	94.17 (94)	114.32 (114)

Using EasyCast and ProCAST softwares to simulate the casting flow field, solidification process, and defects, respectively, as shown in Figs. 8 and 9, it can be seen the casting built by the machine learning model fills smoothly. The length and distribution of the velocity vectors in Fig. 10 are relatively regular, with small changes in magnitude and direction. Therefore, the casting is smoothly filled throughout the process, and there is no turbulence in the cavity. This

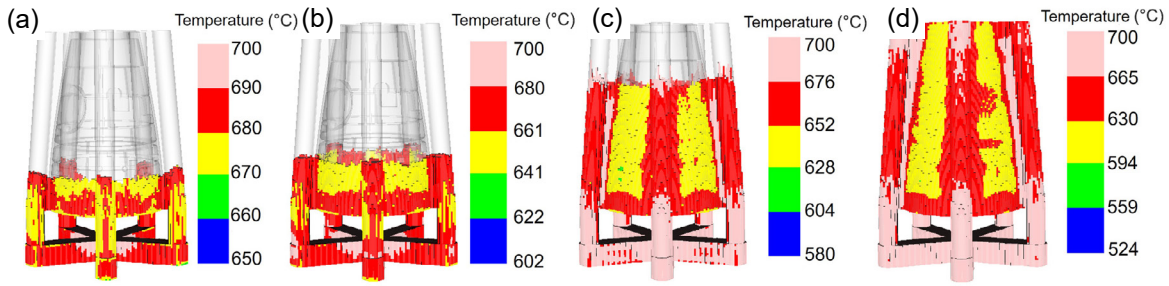

Fig. 8: Simulation results of flow field in EasyCast: (a) filling 40%; (b) filling 60%; (c) filling 80%; (d) filling 100%

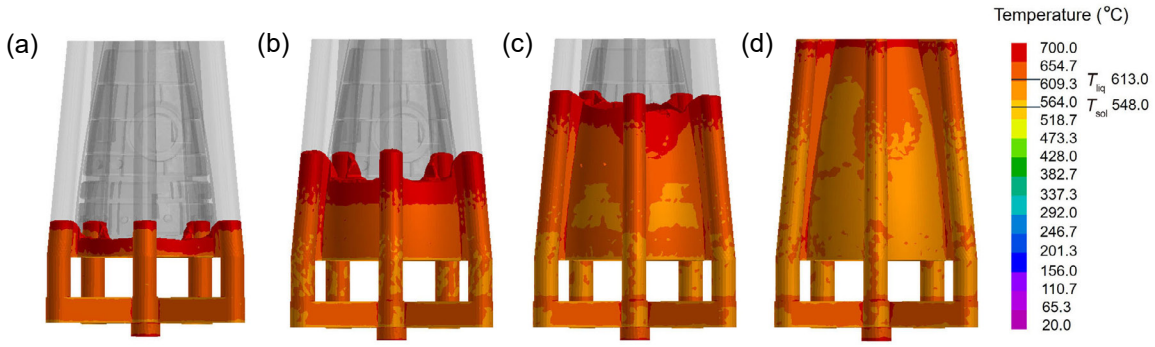

Fig. 9: Simulation results of flow field in ProCast: (a) filling 40%; (b) filling 60%; (c) filling 80%; (d) filling 100%

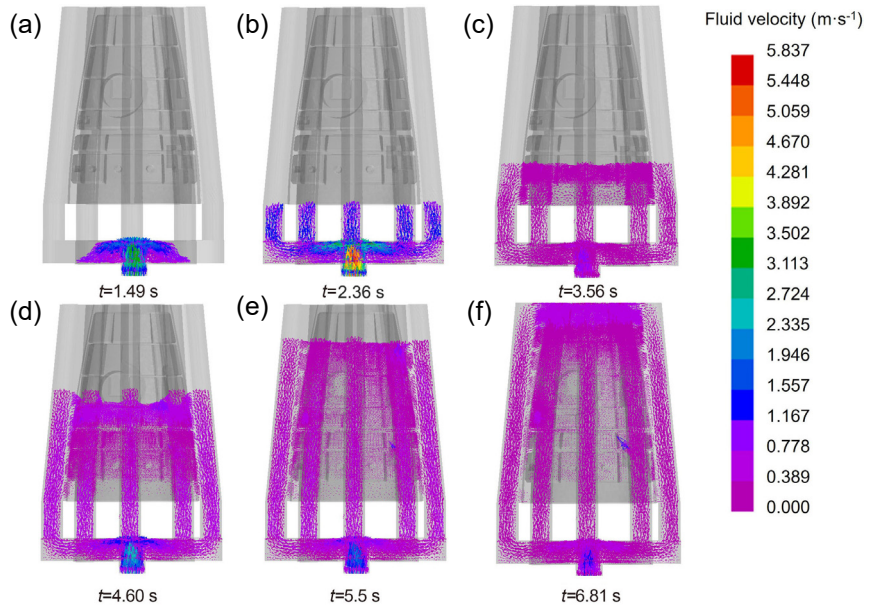

Fig. 10: Velocity vector analysis during the filling process (a–f) showing the velocity vector distribution for different filling times

smooth filling process effectively prevents the alloy liquid from experiencing secondary pumping and the formation of oxidized inclusions. In Figs. 11–12, the solidification sequence is essentially the same for castings, as well as gating systems, simulated using different softwares. The solidification process of the casting begins at the thin wall adjacent to the inner gate and concludes at the gap gating, ensuring smooth filling and unobstructed solidification channels.

Figures 13–14 show the shrinkage cavities distribution of castings designed using two different methods. Figures 13(a) and 14(a) display the defect distribution in castings with gating systems designed using the empirical method, while Figs. 13(b) and 14(b) show the defect distribution in castings with gating systems optimized using the machine learning model.

It can be seen that Figs. 13(b) and 14(b) show fewer shrinkage cavities, which are mainly concentrated within the casting, with smaller shrinkage cavities observed in the internal regions and at the boss areas. Reducing the number of sprue channels results in a more centralized flow path for the liquid metal and reduced flow resistance. In addition, increasing the diameter of the inner gate allows the liquid metal to enter the cavity more uniformly. As a result, the temperature distribution in the cavity becomes more even. This contributes to creating

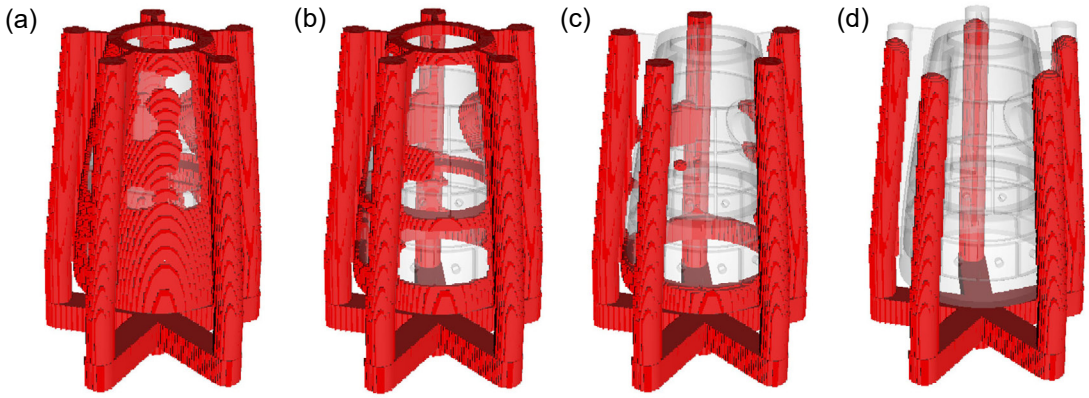

Fig. 11: Solidification results of flow field in EasyCast: (a) solidification 10%; (b) solidification 30%; (c) solidification 50%; (d) solidification 70%

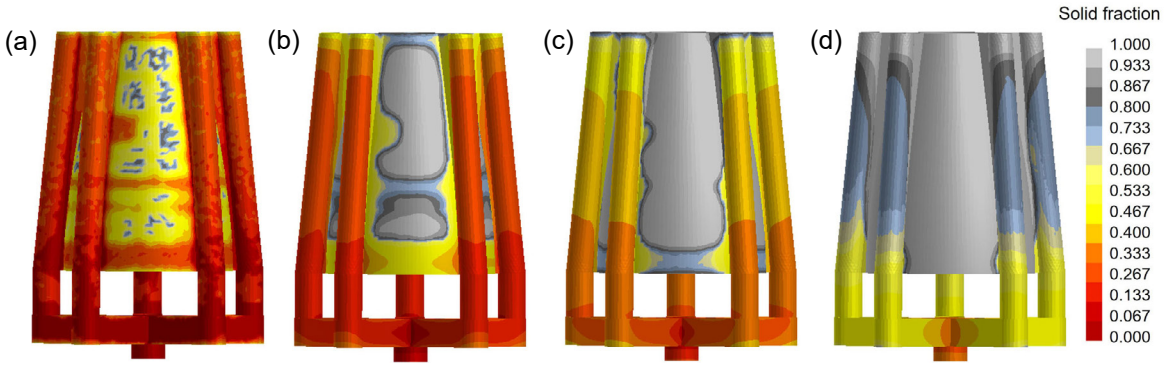

Fig. 12: Solidification results of flow field in ProCAST: (a) solidification 10%; (b) solidification 30%; (c) solidification 50%; (d) solidification 70%

more consistent solidification conditions. Additionally, increasing the diameter of the straight sprue not only improves flow but also enhances shrinkage feeding. More liquid metal can be supplied during solidification, thus reducing the formation of shrinkage porosity.

The results in Figs. 13 and 14 indicate that both EasyCast and ProCAST softwares predict the formation of shrinkage holes at approximately the same locations, with a similar defect distribution. Therefore, the reliability of the machine-learning-designed gating system was verified by using both EasyCast and ProCAST, and the results demonstrate that the machine-learning-designed gating system can reduce shrinkage.

3.3 Optimization process and result analysis

To reduce the formation of shrinkage cavities, ensure higher casting quality, and meet product performance requirements, the optimization focuses on the two main areas where shrinkage cavities are concentrated: the internal regions and the boss areas. Based on the simulation results of the initial design, the addition of internal cooling channels is prioritized to improve the solidification process by enhancing heat dissipation and ensuring more uniform cooling. As shown in Fig. 15, the shrinkage cavities within the casting are eliminated after incorporating the internal cooling channels.

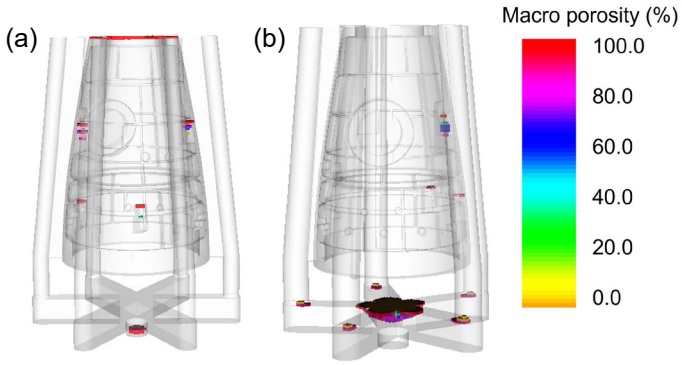

Fig. 13: Defects in different gating systems simulated using EasyCast: (a) empirical formula approach; (b) machine learning models

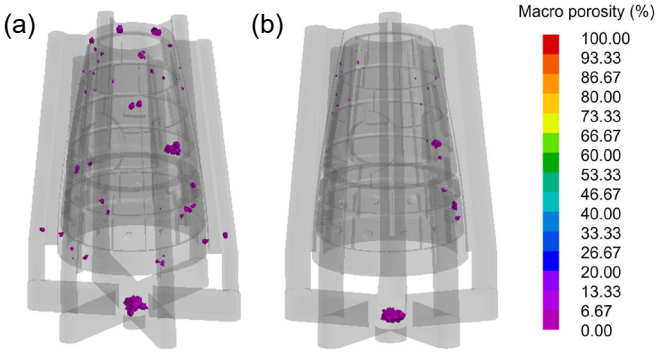

Fig. 14: Defects in different gatting systems simulated using ProCast: (a) empirical formula approach; (b) machine learning models

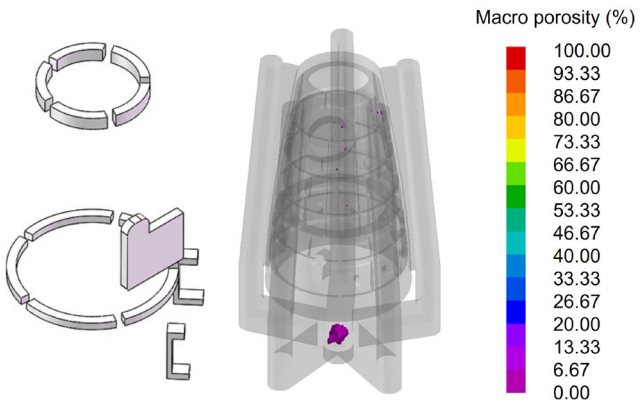

Fig. 15: Defect distribution after design and optimization of internal chill

4 Impact of different inputs on outputs based on machine learning

4.1 Correlations between different features

Correlation analysis is an important step in the feature selection process to assess the degree of association between features and target variables. For machine learning models, the correlation between different features can also be assessed. Since the features do not have a linear relationship with each other, Spearman correlation was chosen to analyze the correlation between different features, as shown in the Fig. 16.

The correlation between the different features can be derived by the Spearman correlation shown in Fig. 16, which takes a value between −1 and 1. The magnitude of the value represents the degree of correlation, and the closer the value is to 1 means the higher the positive correlation between the two covariates, while the moderate correlation level ±0.75 is considered as the threshold value [33]. In the illustration, the correlation between filling time and filling pressure is −0.92, which exceeds the threshold value. Therefore, the features with high correlation need to be eliminated, and between filling time and filling pressure, only one should be retained.

For machine learning input features, the more representative the screened features are, the closer the correlation between different features is to 0. As shown in Fig. 16, the filling time has minimal impact on the defect volume. Only the filling pressure exhibits a positive correlation with the defect volume. This correlation can be attributed to the fact that increased filling pressure causes turbulence in the metal liquid during the filling process, consequently leading to an increase in defect volume.

4.2 Effect of input features on individual output features

Given the non-normal nature of the data, Spearman correlation analysis was chosen for feature selection to study the effect of input features on output features. As shown in Figs. 17–19, the degree of correlation between different input features and each output feature ranges from −1 to 1. A value closer to 1 indicates a stronger positive correlation, while a value closer to −1 indicates a stronger negative correlation.

The gating system parameters are influenced by multiple factors, with each feature having a different impact on the output characteristics. As shown in Figs. 17–19, for this machine learning model, the casting volume has the greatest influence on the gating system, followed by the defect volume, which is negatively correlated. This analysis indicates that

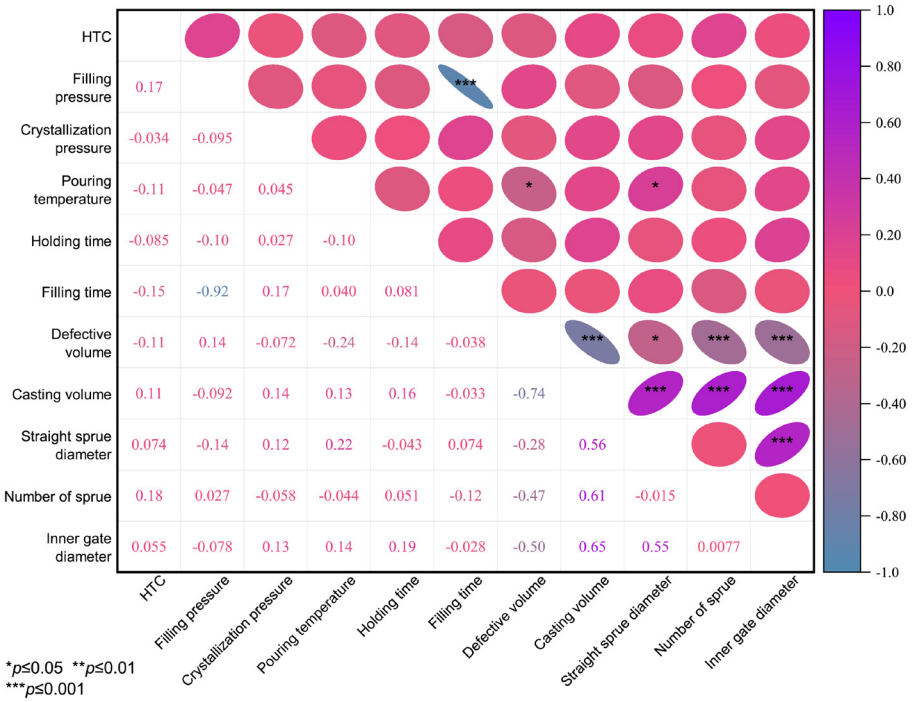

Fig. 16: Spearman correlation coefficient matrix plot, where purple represents positive correlation, blue represents negative correlation; the flatter the ellipse, the larger the value; asterisks (*) indicate significance, determined based on significance levels, displaying *, **, and * for *p*-values less than 0.05, 0.01, and 0.001, respectively**

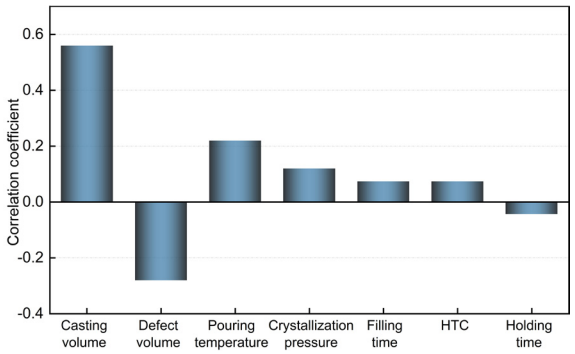

Fig. 17: Correlation between input features and size of straight sprue

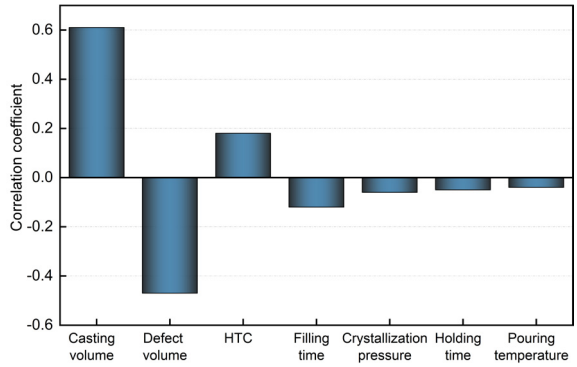

Fig. 18: Correlation between input features and number of sprues

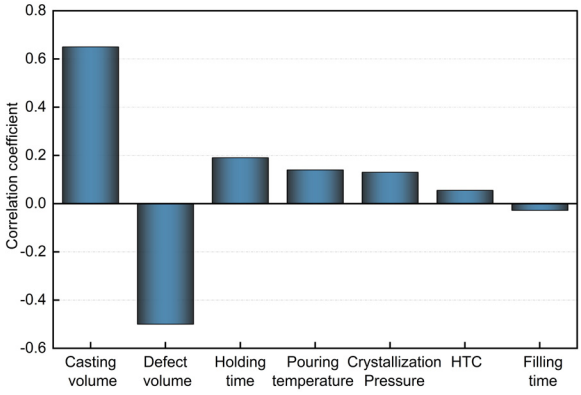

Fig. 19: Correlation between input features and size of inner gate

when the size of gating system is increased, the value of the defect volume decreases. This is because that increasing the gating system size will make the liquid metal filling smoother, thus reducing defects, assuming the process parameters are kept constant. In Fig. 17, the holding time feature has the least influence on the sprue size. In Fig. 18, the pouring temperature has the least influence on the number of sprues. In Fig. 19, the filling time has the least effect on the inner gate dimensions.

5 Conclusions

A prediction model for the dimensions design of gating system was developed using machine learning, with a dataset constructed based on empirical design and numerical simulations. The dataset was then rigorously tested and analyzed using orthogonal tests to ensure comprehensive evaluation. Spearman correlation analysis was applied to identify high-quality data, thereby enhancing the model's accuracy. The flow field, solidification process, and shrinkage distribution were compared and analyzed using EasyCast and ProCAST software for gating systems designed by the empirical method and those optimized by the machine learning model. The model's performance was evaluated using MSE and R^2. The following conclusions can be drawn:

(1) The prediction accuracies for the dimensions of the gating system, based on the machine learning model, are 0.982, 0.856, and 0.820. The specific dimensions of the gating system for the prediction model are as follows: the diameter of the straight sprue is 114 mm, the number of sprue is 5, and the diameter of the inner gate is 94 mm.

(2) The gating system established by the machine learning model can achieve smooth mold filling, top-down sequential solidification, resulting in smaller shrinkage cavities. It indicates that this method is suitable for the design of gating systems of counter pressure casting and facilitates the development of intelligent design strategies in casting processes.

(3) There are slight differences in quantities of shrinkage cavities predicted by the two methods (empirical design method and machine learning model) when analyzed using EasyCast and ProCAST software, but the overall distribution of the shrinkage cavities is similar.

Acknowledgments

This study was supported by the National Natural Science Foundation of China (Nos. 52074246, 52275390, 52375394), the National Defense Basic Scientific Research Program of China (No. JCKY2020408B002), and the Key R&D Program of Shanxi Province (No. 202102050201011).

Conflict of interest

Prof. Yu-hong Zhao is an EBM of *CHINA FOUNDRY*. She was not involved in the peer-review or handling of the manuscript. The authors have no other competing interests to disclose.

References

[1] Zhao Y H, Niu X F, Hou H. Numerical simulation of temperature field during squeeze casting solidification process based on FDM/FEM. Ordnance Material Science and Engineering, 2011, 34(5): 1–4.

[2] Yan Q S, Yu H, Xu Z F, et al. Effect of holding pressure on the microstructure of vacuum counter-pressure casting aluminum alloy. Journal of Alloys and Compounds, 2010, 501(2): 352–357.

[3] Hou Y Y, Wu M W, Huang F, et al. Defect band formation in high pressure die casting AE44 magnesium alloy. China Foundry, 2022, 19(3): 201–210.

[4] Hou H. Macro and micro simulation of filling and solidification process and engineering application in casting technology. Doctoral Dissertation, Taiyuan: North University of China, 2005: 30–35. (In Chinese)

[5] Chen L W, Zhao Y H, Wen Z Q, et al. Modelling and optimization for heat treatment of Al-Si-Mg alloy prepared by indirect squeeze casting based on response surface methodology. Materials Research-Ibero-American Journal of Materials, 2017, 20(5): 1274–1281.
[6] Kang J W, Liu B L, Jing T, et al. Intelligent casting: Empowering the future foundry industry. China Foundry, 2024, 21(5): 397–408.
[7] Zhao Y H. Understanding and design of metallic alloys guided by phase-field simulations. npj Computational Materials, 2023, 9(1): 94.
[8] Zhao Y H, Xin T Z, Tang S, et al. Applications of unified phase-field methods to designing microstructures and mechanical properties of alloys. MRS Bulletin, 2024: 1–13.
[9] Zhao Y H. Integrated unified phase-field modeling (UPFM). MGE Advances, 2024, e44.
[10] Guo R G. Design of gating and feeding system for lowpressure casting based on data-driven. Master's Dissertation, Harbin: Harbin Institute of Technology, 2022: 30–40. (In Chinese)
[11] Papanikolaou M, Pagone E, Jolly M, et al. Numerical simulation and evaluation of campbell running and gating systems. Metals, 2020, 10(1): 68.
[12] Jiang M Q, Chen S, Qi B, et al. Design of investment casting pouring system for support partsbaseoon ProCAST. Computer & Digital Engineering, 2023, 51(4): 978–982.
[13] Wang Y H, Su X P. Study on low pressure casting process design of aluminum alloy thin wall parts. Foundry, 2022, 71(8): 990–993. (In Chinese)
[14] Andrzej K, Jarosz R. Gating system optimization for EV31A magnesium alloy engine body sand casting. Materials, 2022, 15(13): 4620.
[15] Duan Z Q, Chen W P, Pei X L, et al. A multimodal data-driven design of low pressure die casting gating system for aluminum alloy cabin. Journal of Materials Research and Technology, 2023, 27: 2723–2736.
[16] Fu Y J. On the application and development of aluminum alloy casting process optimization technology. Equipment Manufacturing Technology, 2022, 2: 243–245, 252. (In Chinese)
[17] Shan J L, Yi J X, Xu Z F, et al. Production of ZL114A alloy shell castings by low pressure casting. Special Casting & Nonferrous Alloys, 2018, 38(8): 856–859. (In Chinese)
[18] Brůna M, Galcik M, Pastircak R, et al. Effect of gating system design on the quality of aluminum alloy castings. Metals, 2024, 14(3): 312.
[19] Hong R Z, Zhou Y J, Yao W B. Study on pouring system design method of large dementional complicate aluminium precision castings with barrel structure. Journal of Aeronautical Materials, 2006(4): 43–45.
[20] Su Y J, Fu H D, Bai Y, et al. Progress in materials genome engineering in China. Acta Metallurgica Sinica, 2020, 56(10): 1313–1323.
[21] Dong F H, Tao Z H, Sheng W C, et al. Recent progress in the machine learning-assisted rational design of alloys. International Journal of Minerals, Metallurgy and Materials, 2022, 29(4): 635–644.
[22] Zhou D H, Kang Z Y, Yang C, et al. A novel approach to model and optimize qualities of castings produced by differential pressure casting process. International Journal of Metalcasting, 2022, 16(1): 259–277.
[23] Yu J P, Wang D H, Li D Y, et al. Engineering computing and data-driven for gating system design in investment casting. International Journal of Advanced Manufacturing Technology, 2020, 111(3–4): 829–837.
[24] Wang T, Shen X, Zhou J X, et al. Optimal gating system design of steel casting by fruit fly optimization algorithm based on casting simulation technology. International Journal of Metalcasting, 2019, 13(3): 561–570.
[25] Guo Q W, Pan Y, Hou H, et al. Predicting the hardness of high-entropy alloys based on compositions. International Journal of Refractory Metals and Hard Materials, 2023, 112: 106116.
[26] Zhang X Y, Dong R F, Guo Q W, et al. Predicting the stacking fault energy in FCC high-entropy alloys based on data-driven machine learning. Journal of Materials Research and Technology, 2023, 26: 4813–4824.
[27] Zhao W C, Zhen C, Xiao B, et al. Composition refinement of 6061 aluminum alloy using active machine learning model based on Bayesian optimization sampling. Acta Metallurgica Sinica, 2023, 26: 4813–4824.
[28] Chen L Q, Zhao Y H. From classical thermodynamics to phase-field method. Progress in Materials Science, 2022, 124: 100868.
[29] Zhao Y H, Liu K X, Hou H, et al. Role of interfacial energy anisotropy in dendrite orientation in Al-Zn alloys: A phase field study. Materials & Design, 2022, 216: 110555.
[30] Pei X L, Zhao Y H, Chen L W, et al. Robustness of machine learning to color, size change, normalization, and image enhancement on micrograph datasets with large sample differences. Materials & Design, 2023, 232: 112086.
[31] Du X C, Hong R Z, Chen B F, et al. System design of aluminum alloy castings slit gating. Special Casting & Nonferrous Alloys, 2014, 34(7): 767–769. (In Chinese)
[32] Jiang B J. Special casting. Vol. 6, edited by the Foundry Institution of Chinese Mechanical Engineering Society, Beijing: Mechanical Industry Press, 2011: 505–510. (In Chinese)
[33] Duan Z Q, Pei X L, Guo Q W, et al. Design of new Al-Si-Mg alloys by multi-modal mixed inputsimulation experiment. Acta Physica Sinica, 2023, 72(2): 313–323.
[34] Tao Y F, Jiang J G, Fang W. Integrated navigation algorithm based on GRU cyclic neural network. Computer Engineering and Design, 2021, 42(2): 370–376.
[35] Del N G, Pluda A, Pozzetta M. Degenerate elastic networks. The Journal of Geometric Analysis, 2021, 31(6): 6128–6170.
[36] Liu B L, Hu J J, Xie L L. Ranking and comparison of ground motion parameters based on elastic net regression. Journal of Harbin Institute of Technology, 2024, 56(1): 54–62.